SANDIA REPORT
SAND2009-6344
Unlimited Release
Printed September 2009

Final LDRD report: The Physics of 1D and 2D Electron Gases in III-Nitride Heterostructure NWs

George T. Wang, A. Alec Talin, Qiming Li, François Léonard, Bryan M. Wong, Eugenia T. Morales, Andrew Armstrong, Ilke Arslan, Rohit Prasankumar, Prashanth Upadhya, Yong Lin.

Prepared by
Sandia National Laboratories
Albuquerque, New Mexico 87185 and Livermore, California 94550

Sandia is a multiprogram laboratory operated by Sandia Corporation,
a Lockheed Martin Company, for the United States Department of Energy's
National Nuclear Security Administration under Contract DE-AC04-94AL85000.

Issued by Sandia National Laboratories, operated for the United States Department of Energy by Sandia Corporation.

Available to DOE and DOE contractors from
U.S. Department of Energy
Office of Scientific and Technical Information
P.O. Box 62
Oak Ridge, TN 37831

Telephone: (865) 576-8401
Facsimile: (865) 576-5728
E-Mail: reports@adonis.osti.gov
Online ordering: http://www.osti.gov/bridge

Available to the public from
U.S. Department of Commerce
National Technical Information Service
5285 Port Royal Rd.
Springfield, VA 22161

Telephone: (800) 553-6847
Facsimile: (703) 605-6900
E-Mail: orders@ntis.fedworld.gov
Online order: http://www.ntis.gov/help/ordermethods.asp?loc=7-4-0#online

SAND2009-6344
Unlimited Release
Printed September 2009

Final LDRD Report: The Physics of 1D and 2D Electron Gases in III-Nitride Heterostructure NWs

George T. Wang, Qiming Li, Yong Lin
Advanced Materials Science

Andrew Armstrong
Semiconductor Materials & Device Sciences

Sandia National Laboratories
Albuquerque, New Mexico 87185-1086

A. Alec Talin, François Léonard, Bryan Wong, Eugenia T. Morales, Ilke Arslan

Sandia National Laboratories
Livermore, CA 94550

Rohit Prasankumar, Prashanth Upadhya

Center for Integrated Nanotechnologies, Los Alamos National Laboratory
Los Alamos, NM 87185

Abstract

The proposed work seeks to demonstrate and understand new phenomena in novel, freestanding III-nitride core-shell nanowires, including 1D and 2D electron gas formation and properties, and to investigate the role of surfaces and heterointerfaces on the transport and optical properties of nanowires, using a combined experimental and theoretical approach. Obtaining an understanding of these phenomena will be a critical step that will allow development of novel, ultrafast and ultraefficient nanowire-based electronic and photonic devices.

Acknowledgments

We acknowledge support from the Department of Energy Basic Energy Sciences and Sandia's and Los Alamos National Laboratory's Laboratory Directed Research and Development programs. Sandia is a multiprogram laboratory operated by Sandia Corporation, a Lockheed Martin Company, for the United States Department of Energy's National Nuclear Security Administration under contract No. DE-AC04-94AL85000. Los Alamos National Laboratory, an affirmative action equal opportunity employer, is operated by Los Alamos National Security, LLC, for the National Nuclear Security administration of the U.S. Department of Energy under Contract No. DE-AC52-06NA25396.

Table of Contents

List of Figures

1. Introduction

Intense efforts to synthesize and characterize carbon nanotubes and semiconductor nanowires (NWs) in recent years have been due in part to interest in one dimensional (1D) electron systems. 1D electron systems have exhibited many novel properties, including ballistic transport and conductance quantization, and could serve as the basis for new classes of ultrafast and ultraefficient nanodevices. Many open scientific questions remain about the role of electron interactions in 1D, the impact of phonon, impurity, and piezoelectric scattering, and the crossover from 1D to 2D. Additionally, in NWs, where surface atoms comprise a significant fraction of the structure, the surface interface is likely to play a strong role on the transport and optical properties but is currently poorly understood.

In this project, we proposed a new approach where confinement originates from the formation of a 1D or 2D electron gas (1DEG or 2DEG) in a free-standing core-shell semiconductor NW. We proposed to use these novel III-nitride core-shell NWs to examine the currently unknown physics of one-dimensional and two-dimensional electron gases formed in free-standing semiconductor NWs. Additionally, these heterostructure NWs allow us to investigate the role of surfaces and heterointerfaces on the transport and optical properties of NWs, by comparison of GaN NWs with and without shell layers. Obtaining an understanding of these phenomena will be a critical step towards the development of ultrafast and ultraefficient NW-based electronic and photonic devices. Specifically, our primary focus is on Al(Ga)N/GaN core-shell NWs, as the high mobility and breakdown fields of GaN have prompted great interest in the two-dimensional electron gas properties of AlGaN/GaN planar heterostructures for high power and high mobility devices. By exploiting our ability to vary the diameter of the NW core and composition of the shell, it should be possible to effects of size, band-gap engineering, and piezoelectric effects on the 1DEG and to examine the transition to 2DEG behavior. The experimental studies are complemented by theoretical modeling in order to understand and predict the electronic structure of nature of the electron gases formed in these novel structures.

2. Technical Approach

Our approach is based on III-nitride core-shell heterostructure NWs as model systems for investigating the formation and physics of 1DEGs and 2DEGs in semiconductor nanostructures

and for understanding how surface and interface issues affect the electrical transport and optical properties of semiconductor NWs. We have recently demonstrated the growth of single-crystal GaN NWs and core-shell radial heterostructure NWs consisting of GaN cores and various III-nitride shells, including AlN, AlGaN, InGaN, and InN, via vapor-liquid-solid (VLS) Ni-catalyzed metal organic chemical vapor deposition (MOCVD). Further details of the growth can be found elsewhere.*[1-5]* For this work, we synthesized GaN, AlGaN/GaN, and AlN/GaN core-shell NWs with varied diameters and shell thicknesses. By comparing the properties of GaN NWs with and without shell layers, the effects of surface passivation and potential electron gas formation can be studied. The structure and composition of the NWs heterostructures, which will have a critical influence on the electron gas and electronic properties, were investigated by high resolution scanning electron microscopy (SEM) and scanning transmission electron microscopy (STEM), along with 3D STEM tomography. The composition and optical properties of the NWs were probed via micro-photoluminescence (μ-PL), electron dispersive spectroscopy (EDS), and nano-cathodoluminescence (CL) measurements. Defect states were investigated using deep-level optical spectroscopy (DLOS). Ultrafast optical measurements were also employed to study carrier dynamics in the NWs. Further experimental details can be found in the Results section.

Room temperature transport properties of the NWs were investigated by leveraging a platform we have recently developed at Sandia allowing for the combined electrical and optical characterization of large numbers of NWs.*[6]* In order to observe evidence of electron gas formation in the core-shell NWs by evidence of enhanced mobilities, the NW-based architectural equivalent of a high-electron mobility transistor (HEMT, or modulation doped field-effect transistor, or MODFET) was fabricated using this platform. For the device gate we employed a back-gating scheme, using the Si/SiO_2 substrate, as well as a top-gate structure, which ideally should provide stronger gate coupling.

Theoretical modeling was also undertaken in order to discern the structure of electron gases formed in these novel NWs. Specifically, the goals were to: (1) explore the parameter space and identify the conditions under which a 1DEG/2DEG might be expected; (2) understand the detailed electronic properties of the electron gas; (3) model in detail the properties of the particular structures realized experimentally. The theoretical modeling used a self-consistent Poisson-Schrödinger approach couple to finite-element modeling applicable to any core/shell

NW geometry, including the triangular geometry relevant to current experiments in this project. Spontaneous and piezoelectric polarization effects relevant to the III-nitrides were also incorporated into our models.

3. Experimental Details & Results

3.1. Synthesis & structural characterization of GaN & Al(Ga)N/GaN NWs

GaN NWs as well as AlGaN/GaN, and AlN/GaN core-shell NWs were grown by Ni-catalyzed MOCVD. Unintentionally doped (UID) GaN NWs were grown via MOCVD on *r*-plane sapphire using a thin (2 nm) Ni film deposited by e-beam evaporation as the catalyst for vapor-liquid-solid (VLS) growth, as previously described.*[3-5]* Growth proceeded for 5 minutes at a substrate temperature of 900 °C and a pressure of 75 Torr. III-V growth precursor flows were 95 standard cubic centimeters per minute (sccm) H_2 through a trimethylgallium (TMGa) bubbler at a temperature of 20 °C and 16,000 sccm ammonia (NH_3). These growth conditions yielded highly-aligned NWs grown along the $[11\bar{2}0]$ direction with single crystallinity, wurtzite structure and triangular cross-sections with a $\{0001\}$ facet and two equivalent $\{1\bar{1}01\}$ facets.*[5]* Ga-(0001) versus N-(000-1) polarity for $\{0001\}$ facet of the NWs here has not been determined, though N-polarity has been established for MOCVD-grown VLS triangular GaN NWs grown also along $[11\bar{2}0]$.*[7]* One NW set included GaN NWs (ID: 070928A), while the other sets consisted of NWs grown under nominally the same conditions, followed by *in-situ* epitaxial growth of an AlGaN (ID: 071214A) or AlN (071214B) shell. For the *in-situ* growth of the AlGaN shell, the growth temperature was increased to ~1050 °C and the growth was carried out for 30 seconds at 75 Torr. The trimethylaluminum (TMAl) flow rate was set to 45 sccm using a bubbler maintained at a temperature of 25 °C. For TMGa, a flow rate of 90 sccm was used with the bubbler at a temperature of -5 °C and the NH_3 flow rate was set to 2400 sccm. For the growth of the AlN shell, the TMAl and NH_3 flow rates were set to 50 sccm and 2000 sccm, respectively, and the growth was carried out at 1050 °C and 75 Torr for 66 seconds.

Of this initial set of NWs, an AlGaN/GaN NW sample (ID: 071214a) was selected for further structural characterization. In order to determine the thickness and approximate Al concentration of the AlGaN shell layer, scanning transmission electron microscopy (STEM) and high

resolution TEM (HR-TEM) were performed on the AlGaN/GaN core-shell NWs. Cross-section views of the NW were found to be necessary to distinctly image the GaN core and AlGaN shell layer. Cross-section TEM samples were prepared by dispersing the NWs flat onto a gold-coated Si substrate, followed by focused ion beam milling cross-section slices of the silicon, an example of which is shown in the TEM image in Figure 1a. HR-TEM experiments on these samples indicate that core and shell layers are single crystalline wurtzite, as shown in Figure 1b. Because the interface between the GaN core and AlGaN shell was not unambiguous in the HR-TEM images, high z-contrast STEM experiments were performed to image and measure the thickness of the AlGaN shell layer. The STEM image in Figure 1c shows a distinct $Al_{0.3}Ga_{0.7}N$ shell layer roughly 2.5 nm thick, where the Al content was determined by EDS.

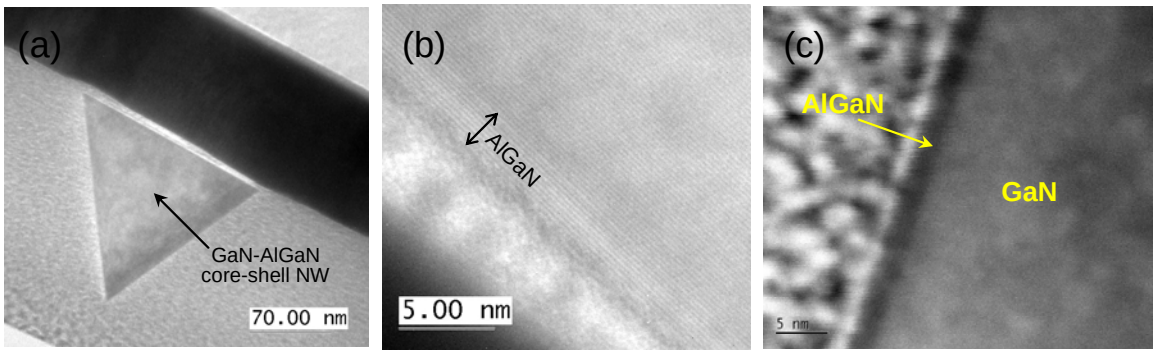

Figure 1. (a) TEM image of a GaN-AlGaN core-shell NW cross-section. (b) HR-TEM and (c) STEM images showing AlGaN shell layer approximately 2.5 nm thick surrounding the GaN NW core.

Because this 2.5 nm thick AlGaN layer is likely too thin to sustain electron gas formation, additional AlGaN/GaN NW samples were grown with targeted thicker AlGaN shell layers. Figure 2a shows STEM cross-section images of two AlGaN/GaN NWs (ID: 080331B) with thicker AlGaN layers. We noted variations of the AlGaN thickness on the three different facets of the NWs and also across different NWs from the sample, and STEM analysis of eight cross-sectioned NWs from the sample revealed AlGaN shells ranging from around 4-10 nm in thickness on average. An additional sample (ID: 081103B) was grown with even thicker AlGaN shells (typical AlGaN shell thicknesses ranging from ~8-30 nm) to improve the possibility of electron gas formation at the AlGaN/GaN interface. A NW from this sample is shown in Figure 2b, which has AlGaN shell thicknesses of ~25-35 nm on the different facets. Contrast variations

and EDS analysis also revealed compositional variations in the Al content at different locations in the AlGaN shell layer.

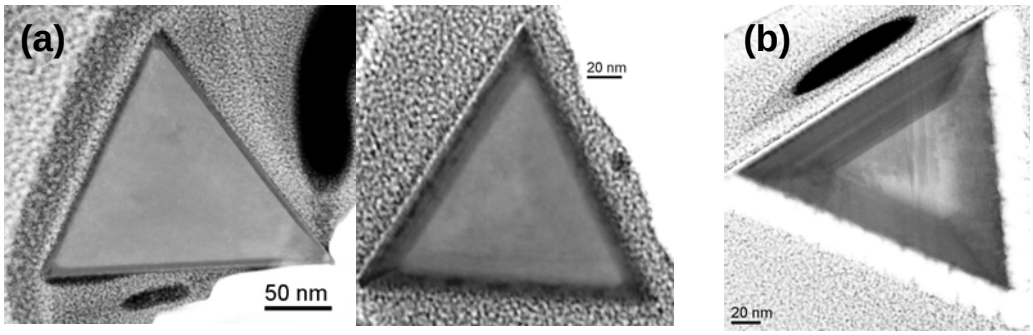

Figure 2. Cross-section STEM images of AlGaN/GaN NWs (a) ID: 080331B with typical AlGaN shell thicknesses ~4-10 nm on average and (b) ID: 081103B with typical AlGaN thickness ~8-30 nm.

We also conducted the first 3D STEM tomography experiments on AlN/GaN core-shell NWs in order to elucidate their true morphology in 3D. This provides a significant advantage to conventional (S)TEM experiments, which are based on 2D projections of a 3D object and can lead to misleading interpretations. This tomographic technique involves reconstructing a tilt/rotation series of STEM images to recreate the 3D morphology of the NW; additional experimental details are given elsewhere.*[2]* Figure 3 shows snapshots of reconstructed tomographs of two AlN/GaN NWs. Significantly, the 3D results show an AlN shell layer ~ 5 nm with good uniformity both along the length of the NW and across all three facets. Additional results have been published elsewhere.*[2]*

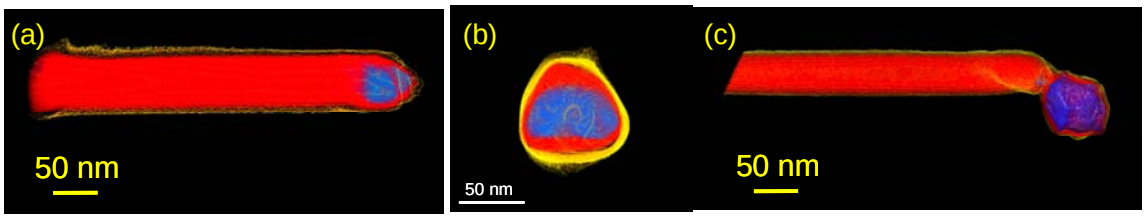

Figure 3. 3D STEM tomography images showing (a) side and (b) front-end views of a GaN-AlN core-shell NW with on-axis Ni catalyst tip. (c) GaN-AlN core-shell AlN NW with off-axis Ni catalyst tip. Red = GaN, Yellow = AlN, Blue = Ni.

3.2 I-V and photoluminescence measurements of GaN & Al(Ga)N/GaN NWs

Large numbers of single NW devices with source and drain contacts were fabricated using a platform we have developed at Sandia consisting of an interdigitated electrode array containing 32 individually addressable electrodes, as shown in Figure 4. This platform allows for the correlated electrical and optical characterization of large numbers of single NW devices. Micro-photoluminescence (μ-PL) spectra for individual NWs were collected using a home-built system, with a 325 nm He–Cd laser focused though a 32× reflective objective, and a CCD camera/spectrometer (OceanOptics™) combination coupled to the electrical probe station microscope. Further details on the device fabrication process and μ-PL setup is described elsewhere.*[6]* μ-PL measurements show a strong dependence of the optical properties of the GaN NWs on temperature, with NWs grown at 900 °C exhibiting a ~30× increase in the intensity of the band-edge luminescence (BEL) at ~365 nm compared to NWs grown at 850 °C, which show a strong yellow luminescence (YL) indicative of defect states centered at ~540 nm. An $I \propto V2$ power law dependence was also observed for NWs grown at the lower temperatures of 800 °C and 850 °C, indicating that electrical transport is dominated by space-charge limited conduction (SCLC).*[8]* The resistivity of the GaN NWs showed a similar dependence on the NW growth temperature, with NW resistivity decreasing roughly four orders of magnitude at 900 °C compared to NWs grown at 850 °C.*[6]* A clear correlation between the optical and electrical properties is seen in Figure 5, where the NW resistivity is plotted versus the integrated BEL intensity normalized by the total integrated luminescence intensity. We believe possible carbon incorporation during growth from the TMGa precursor is responsible for the low BEL intensity and the high resistivity observed at the lower growth temperatures.

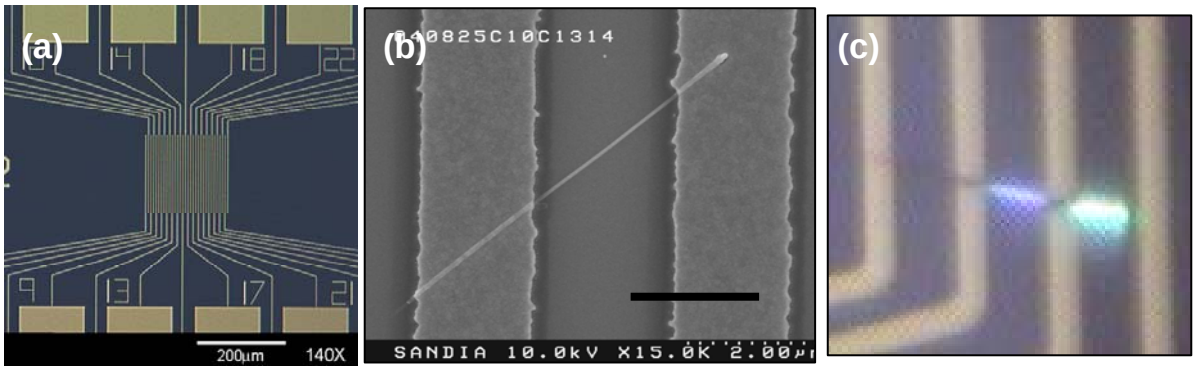

Figure 4. (a) & (b) NW characterization platform comprised of a 32 top-deposited electrode pattern on NWs dispersed on a Si/SiO_2 substrate; (c) μ-PL image on an electrically-contacted NW device.

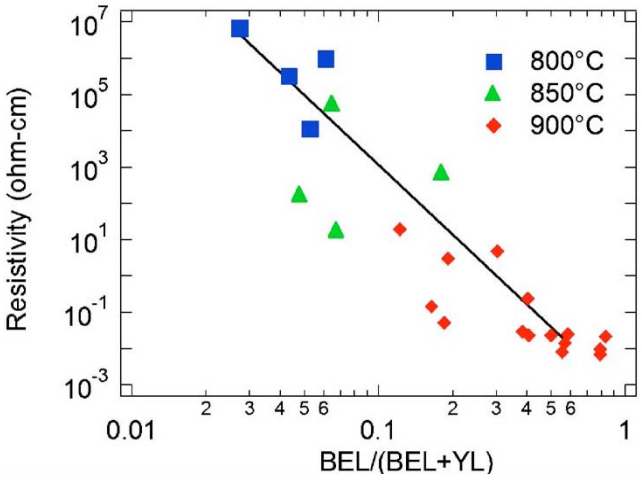

Figure 5. GaN NW resistivity plotted vs. the normalized BEL to (BEL + YL) intensity.

The I-V characteristics of AlGaN/GaN (ID: 071214A) and AlN/GaN (ID: 071214B) core-shell NWs were also probed and compared to those of GaN NWs (070928A) grown under identical conditions for the GaN NW core, and are shown in Figure 6. The preliminary data indicate that both the AlGaN/GaN and AlN/GaN core-shell NWs exhibit reduced resistance in general compared to the GaN NWs at a given mean diameter. Moreover, we observed that a much higher fraction of core-shell NWs are conductive, compared to GaN NWs, where a large number of NWs were not conductive. Thus, the shell layers may be altering or mitigating surface states that cause carrier depletion in the NW bulk*[9]* and lead to reduced conductivity.

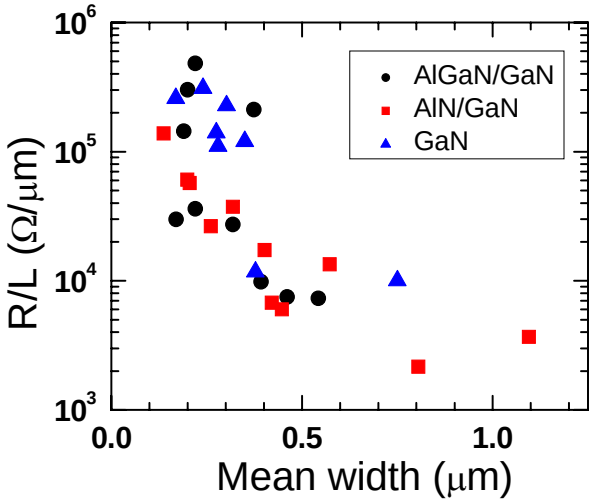

Figure 6. R/L vs. mean width for GaN vs. Al(Ga)N/GaN NWs

3.3 Spatially-resolved cathodoluminescence studies of GaN & Al(Ga)N/GaN NWs

The optical properties of GaN & Al(Ga)N/GaN NWs were also studied with high spatial resolution by cathodoluminescence (CL) experiments. In CL the electron beam-induced excitation is largely localized within the electron beam dissipation volume in the target materials.*[10]* By decreasing the electron beam energy, the electron beam dissipation volume can be reduced to tens of nanometers.*[11]* This allows for significantly improved spatial resolution in comparison with photoluminescence (PL) and μ-PL, which a particular benefit for investigating the optical properties of nanostructures.*[12]* The CL experiments were performed using a Gatan MonoCL2 system equipped with a high-sensitivity GaAs:Cs photomultiplier tube; data were taken at room temperature and ultra high vacuum conditions, at a beam voltage of 2.5 keV

Figure 7a shows a typical SEM image of a group of GaN NWs with diameters ranging from 55 to 460 nm. The NW diameter is defined here as the cross-sectional width of one of the three sides, which are roughly equivalent.*[5]* The same NW group is imaged with CL for near band-edge luminescence (BEL) at 361 nm and YL at 550 nm, as shown in Figure 7b and Figure 7c, respectively. As seen by comparing Figure 7a and Figure 7c, all the NWs imaged exhibit significant YL. However, as seen in Figure 7b, only the larger-diameter NWs exhibit BEL, while the smaller-diameter NWs show no detectable signal near 361 nm. For example, in Figure 7a, Arrow A indicates a GaN NW with a diameter of ~300 nm. Strong BEL and YL signals are detected for this NW as indicated in Figure 7b and Figure 7c. In contrast, on a NW with a dimension of ~75 nm (Arrow B in Figure 7a), any BEL is too weak to be detected (Arrow B in Figure 7b) while strong YL is still measured (Arrow B in Figure 7c). After investigating this luminescence dependence on NW diameter for roughly one hundred GaN NWs, we find that there exists a critical dimension of approximately 80 nm, below which the BEL is not detectable, whereas strong YL is measured at all diameters. This observation can be explained by considering a simple volumetric model that assumes YL arises primarily from the surface region and BEL occurs only in the core region. Based on the geometry of a NW with an equilateral triangle cross-section, at the critical diameter of 80 nm, where BEL is experimentally observed to be “pinched off” for this set of NWs, the YL “shell” is calculated to be ~23 nm thick. Evidence for strong YL at the surface region is also shown by the spatially-resolved CL images in Figure 8.

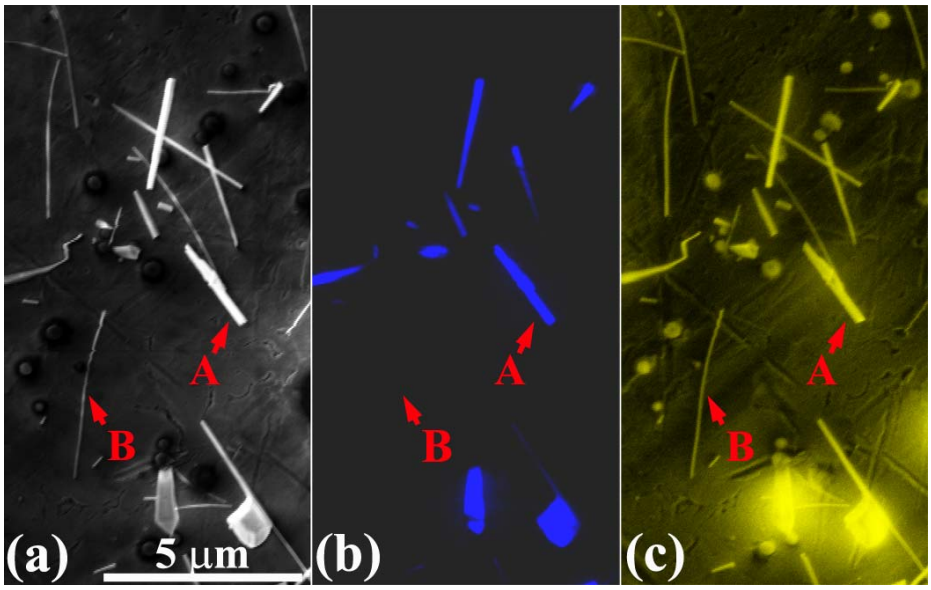

Figure 7. (a) SEM image of GaN NWs with dimension ranging from 55 to 450 nm. (b) CL image of same view showing GaN BEL at 361 nm. (c) CL image showing defect-related YL at 550 nm.

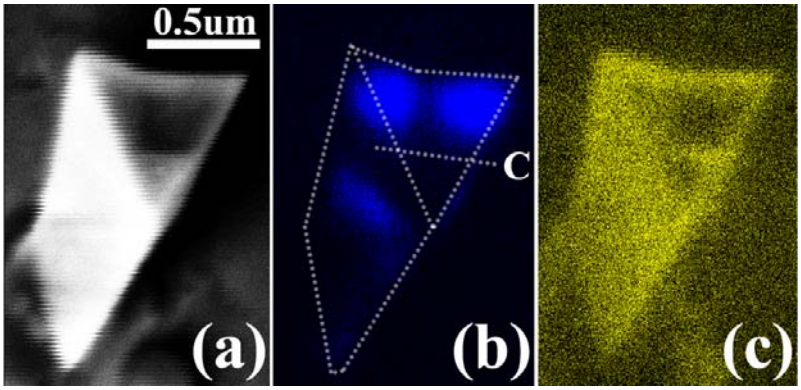

Figure 8. (a) SEM image of a GaN NW with visible cross-section and a sidewall. (b) CL image on GaN showing GaN BEL at 361 nm. (c) CL image showing defect-related YL at 550 nm.

CL experiments on GaN NWs that were post-annealed at high temperature or had an AlGaN shell grown were also studied to investigate potential surface passivation effects on the YL. Figure 9 shows the YL/BEL intensity ratio dependence on NW dimension after the as-grown GaN NW was annealed in NH_3 for 3 minutes at 900°C and after the as-grown NW sidewalls was coated with a ~3-nm-thick AlGaN shell layer. As compared with as-grown GaN NW samples, both the annealed NWs and AlGaN/GaN NWs showed nearly 2 orders of magnitude reduction on YL/BEL

intensity ratio. Moreover, the YL/BEL intensity ratio becomes nearly constant as the NW dimension changes. This result indicates that the YL related defects are no longer as concentrated near the surface of the NWs. We suspect that both annealing and AlGaN shell growth may both lead to termination of the dangling bonds at the GaN NW surface, which could be a source of the surface YL.

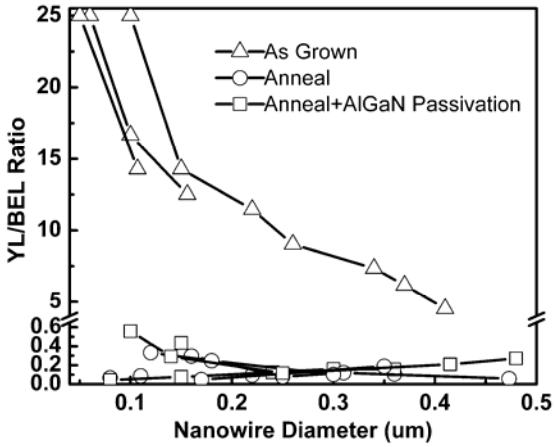

Figure 9. YL/BEL intensity ratio for as grown GaN NWs (triangles), annealed NWs (circles), and AlGaN-passivated core-shell NWs (squares).

3.4 Deep level optical spectroscopy of GaN & Al(Ga)N/GaN NWs

Deep level optical spectroscopy (DLOS)*[13]* was used to compare deep level defects between GaN NWs and AlGaN/GaN core-shell NWs. The deep level spectrum of GaN NWs can be investigated quantitatively by studying sub-band gap PC as a function of the energy of incident monochromatic photons ($h\nu$). Further details of DLOS*[13]* and photoconductivity (PC)-DLOS techniques are given elsewhere.*[14]* The DLOS spectra of the GaN NWs were reported in detail in a recent publication,*[14]* and the GaN NW deep level energies are similar to those reported for thin film GaN,*[15, 16]* suggesting that the associated defect centers are bulk-like in nature and are not related to the NW surface. DLOS spectra of the AlGaN/GaN NWs (ID: 071214A) were found to closely resemble those of the GaN NWs. This finding suggests that the deep level properties of defects in the GaN NW are unaffected by the AlGaN shell, as expected. However, comparison of the PC transients shown in Figure 10 for the GaN and

AlGaN/GaN NWs reveals a deep level that is strongly affected by the AlGaN shell. The negative component in PC transients evident in the GaN NWs for $h\nu$ 2.60 eV was not observed for the AlGaN/GaN NW. This negative PC component was observed for every GaN NW and was absent for every AlGaN/GaN NW investigated, and is thus attributed to a GaN surface-related defect owing to its exclusivity to GaN NWs without an AlGaN shell. A negative component in the *n*-type GaN NW PC transients signifies hole photoemission from a deep level.

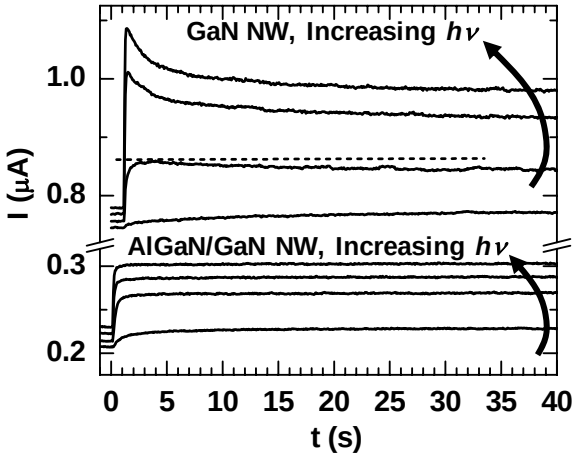

Figure 10. PC transients for the GaN NWs and AlGaN/GaN NWs for $h\nu$ = 2.55 eV, 2.75 eV, 2.925 eV, and 3.125 eV. The dashed line is a guide to the eye emphasizing the negative PC component.

The absence of the E_v + 2.6/E_c – 0.8 eV surface state for the AlGaN/GaN NWs suggests that the epitaxial AlGaN shell mitigates the defect level, potentially through coordination of the dangling Ga bonds of the GaN surface or by shifting the GaN surface state energy below E_F, effectively passivating the defects. The observation and mitigation of a GaN surface state is important for GaN NW-based opto-electronic or sensor devices.

3.5 Ultrafast carrier dynamics in GaN and Al(Ga)N/GaN NWs

Optical pump-probe spectroscopy, arguably the simplest ultrafast optical measurement, can provide a great deal of information on carrier dynamics in these nanosystems. This technique probes the sum of electron and hole distributions at a given photon energy and therefore has the potential to separately measure electron and hole dynamics in semiconductor

nanostructures, contrasting with time-resolved photoluminescence (TRPL) measurements, which measure the product of electron and hole distributions and therefore cannot separately probe electron and hole dynamics.*[17]* Therefore, it can be expected that optical pump-probe measurements on GaN NWs may reveal physics unique to these nanoscale structures, while enabling the measurement of parameters important for nanophotonic applications of NW-based devices. For example, GaN-based devices commonly exhibit "yellow luminescence" (YL), in which a broad luminescence band centered at 550 nm that is believed due to deep acceptor states reduces device efficiency.*[18]*,*[19]* Ultrafast optical spectroscopy can shed light on this problem by measuring carrier transfer into and out of these states, which will be important in understanding this phenomenon and optimizing device performance. The optical pump-probe system used in the experiments on GaN NWs is based on a 100 kHz regeneratively amplified Ti:sapphire laser system (Coherent RegA) producing 50 fs, 10 μJ pulses at 800 nm. Further details are available elsewhere.*[20]*

The motivation for the experiments discussed in this section was therefore to temporally resolve carrier relaxation into and out of the defect states related to YL after above band-gap excitation to gain fundamental insight on this phenomenon.

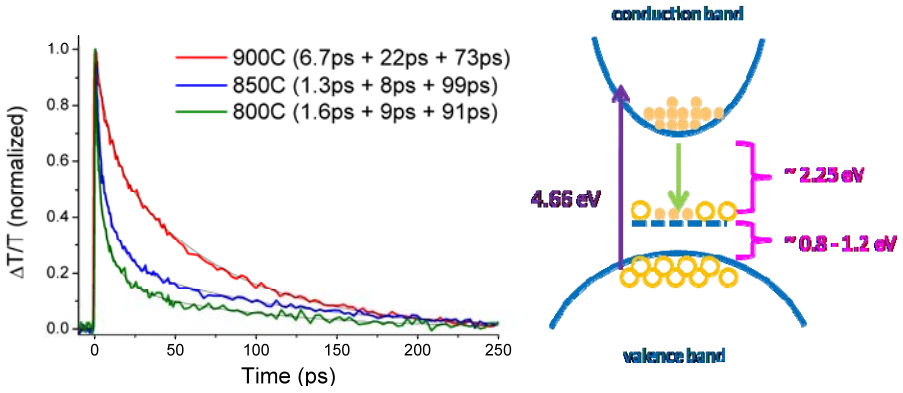

(a) (b)

Figure 11. (a) UV-pump, optical-probe measurements on GaN NWs grown at different temperatures. (b) Schematic band structure of GaN depicting the position of the YL-related defect states, related optical transitions, and electron and hole populations after pump excitation.

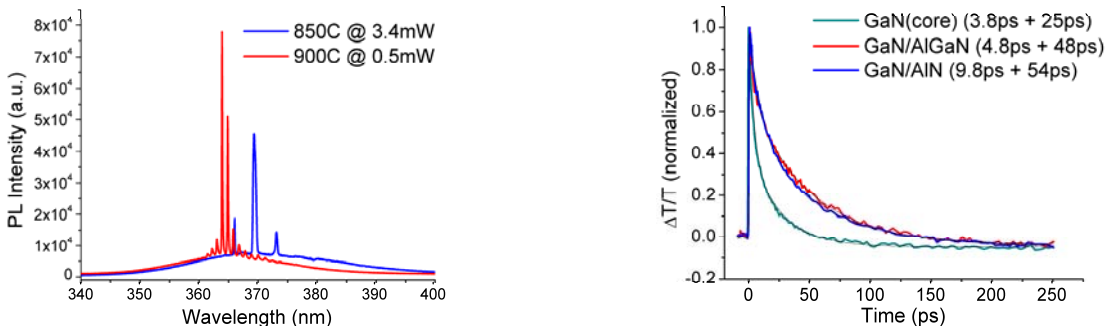

(a) (b)

Figure 12. (a) Band edge PL spectra showing lasing near the threshold pump (266 nm) power. (b) Comparison of carrier relaxation dynamics at 550 nm after 266 nm excitation in GaN core and core-shell structures grown at 900 °C.

We performed UV-pump, optical-probe measurements on GaN NWs grown at T_{sub}=800, 850, and 900 °C, the results of which are shown in Figure 11a. Figure 11b schematically depicts the electron and hole populations following photoexcitation with a 4.66 eV pump pulse, after the photoexcited electrons and holes have thermalized and relaxed to the band minima. A 550 nm (2.25 eV) visible pulse then probes the transition between the conduction band and a mid-gap band of defect states that is believed responsible for YL.*[19]* The rise time of our signals indicates that photoexcited carriers populate the states responsible for YL within ~500 fs, while the long-lived decay due to relaxation out of these states is observed to increase with T_{sub}. Further insight can be obtained from photoluminescence (PL) measurements on these samples.*[21]* These measurements indicate that the concentration of defects responsible for YL remains unchanged with T_{sub}, as evident from the relative intensity invariance of the YL band (not shown), while the band edge luminescence (BEL) intensity is an order of magnitude higher for T_{sub}=900 °C. Therefore, the faster relaxation in NWs with lower T_{sub} may be attributed to the presence of additional impurity sites, possibly due to carbon incorporation from carbon-bearing precursors present during growth, that non-radiatively trap photoexcited carriers into these additional defect states.*[21]* These growth temperature dependent impurity sites can also influence the free carrier concentration and hence the BEL properties of the NWs. This is confirmed by BEL measurements (Figure 12a), which show a decreased lasing threshold for NWs with higher T_{sub}.

Next, we examined AlN/GaN and AlGaN/GaN NWs in order to understand the influence of surface states on carrier relaxation out of the YL-related states. We performed time-resolved UV-pump, visible-probe experiments on GaN NWs without a shell and NWs with AlN/GaN and AlGaN/GaN core-shell structures (Figure 12b). The NWs with shells exhibit a longer relaxation time, independent of the shell composition, which suggests that surface states also contribute to carrier trapping out of YL defect states and that radially heterostructured epilayers can passivate these states. *The results are thus consistent with the I-V measurements, DLOS results, and CL measurements showing that the AlGaN or AlN shells mitigate or passivate surface states in the GaN NWs, resulting in an improvement in their properties.* These are also some of the first ultrafast optical experiments on core-shell NWs.

3.6. AlGaN/GaN NW field-effect transistors

In order to see evidence of electron gas formation at the AlGaN/GaN interface via enhanced mobilities, electrical transport in the AlGaN/GaN core-shell NWs was characterized by fabricating three types of NW field effect transistor (NWFET) structures. The first and simplest structures consisted of randomly dispersed NWs on n-Si/SiO2 (100 nm) substrates, with Ti/Au (20 nm/300 nm) metal contacts defined using optical lithography. The complete process consisted of sonicating a NW growth specimen in isopropanol, followed by spin-coating approximately 1 mL of the resulting suspension onto a slowly rotating Si/SiO2 substrate and allowing the liquid to dry. The wafer was then coated with Futurex negative photoresist and patterned using a Suss MA-6 optical aligner. After development, the wafer was briefly etched in oxygen plasma to remove residual organics. Metal contacts were electron-beam evaporated onto the patterned wafers, followed by lift-off in acetone at room temperature. Sonication was used briefly to help remove the resist during lift-off procedure. Finally, the patterned wafer was cut into smaller pieces, which were annealed in a vacuum furnace at 600 ^{o}C. An Ohmic contact to the Si wafer was fabricated by first scratching with a diamond scribe, followed by application of Ag paste (TedPella). Typically 2 spots were made in this fashion and were characterized by current-voltage measurement to assure that the contact was indeed Ohmic. A schematic of this NWFET structure along with a SEM image, are shown in Figure 13a and Figure 13b, respectively. A second type of structure consisted of a Ni/Au (100 nm/240 nm) Schottky gate

deposited between the Ti/Au source/drain electrodes. This deposition was done after the source/drain electrodes were thermally annealed. A schematic along with a SEM image for the Schottky FET are shown in Figure 13c and Figure 13d, respectively. The gate structure was fabricated using optical lithography by utilizing a mask consisting of half the interdigitated fingers used for the bottom-gate NWFET. The third structure consisted of an alumina insulator deposited using atomic layer deposition prior to top metal gate fabrication. The Al_2O_3 layer was deposited at UC Berkeley (Peidong Yang's group), at 200^{o}C and a thickness of 16 nm, requiring 100 reaction cycles. A schematic for this device structure is shown in Figure 13e.

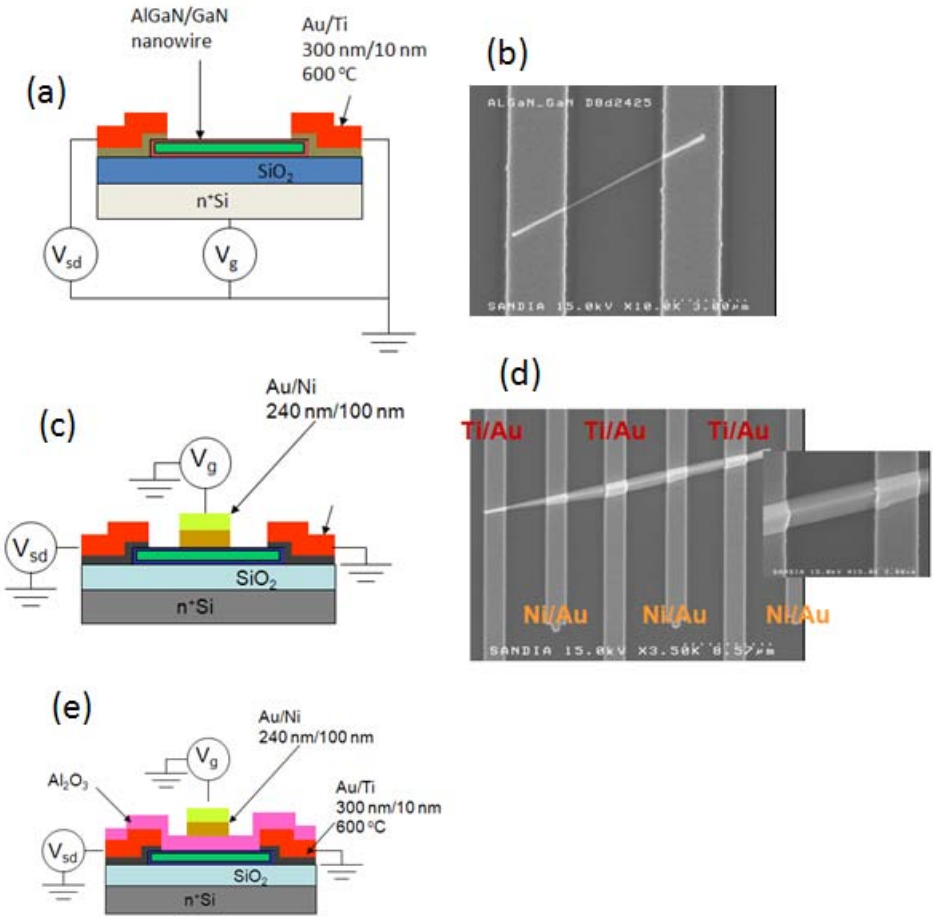

Figure 13. Fabricated NW FET structures

All devices were tested using a home built probe station with computer controlled Keithley 237 meters for gate and source-drain voltage source/current meter functions.

Approximately 10 NWs were tested in the type 1 NWFET configuration. At least three NW specimens showed n-type FET behavior, and could be turned-off at a bias of approximately -7 V. Source-drain current (I_{sd}) versus drain bias (V_{sd}) collected at different gate voltages (V_g), and gate transfer characteristics for one of the devices are shown in Figure 14a and Figure 14b, respectively. Carrier mobility for this NWFET was calculated from the transfer characteristics using equation 1,

$$\mu = \frac{L^2}{CV_{sd}}\left(\frac{dI_{sd}}{dV_g}\right) \qquad (1)$$

Where L is the NW length between the source and drain electrodes and C is the capacitance between the Si electrode and the NW, expressed according to equation 2,

$$C = 2\varepsilon\varepsilon_o \frac{L}{\ln\left(2t/R\right)} \qquad (2)$$

Where t is the oxide thickness (100 nm), R is the NW radius, ε is the relative dielectric constant and ε_o is the permittivity of vacuum. Using the above equations, the NW shown in Fig. 1 has a carrier mobility of 114 cm^2/Vs. Two other NWs displayed similar electrical characteristics, resulting in an average mobility of ~100 cm^2/Vs. Previously, we have found just one GaN NW which displayed sufficient gate dependence, and which yielded a mobility of ~0.1 cm^2/Vs. The higher mobility and stronger gate dependence for the AlGaN/GaN NWs is likely the result of the shell acting to passivate the surface states on the GaN surface, in agreement with recent results by Armstrong et al. on similarly grown NWs.

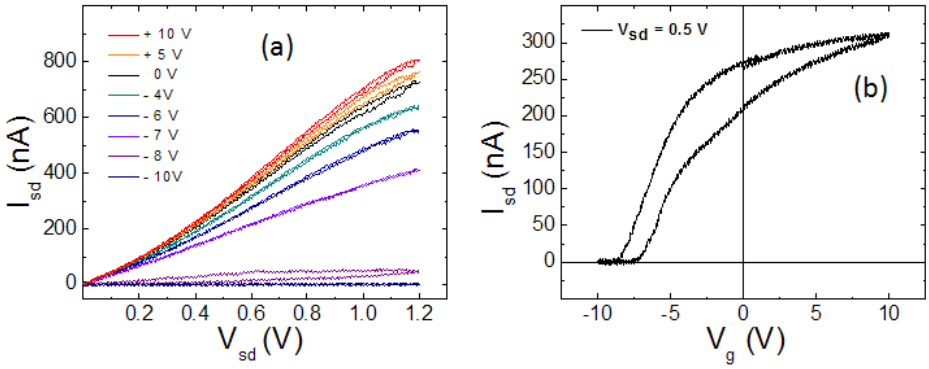

Figure 14. (a) gated I-V measurements; (b) I vs V_g showing hysteresis behavior

Type 2 and type 3 NWFETs (ID: 081103B) were analyzed using the same equipment as was used for type 1 devices. Figure 15 shows I-V characteristics for one of the type 2 devices (Ni/Au Schottky gate). The I-V curves indicate that the FET turns 'ON' at negative bias applied to the gate. This behavior is characteristic of hole carriers in the channel, in contrast to the negatively charged carriers (i.e. electrons) observed for Si bottom gate NWs. At least two devices were observed with similar characteristics. At present, we do not have a clear explanation for these observations, and further experiments and measurements will be necessary.

Type 3 devices (with Al_2O_3 dielectric between the top Ni/Au gate electrode and the NW) exhibited non-linear source-drain I-V characteristics, without strong dependence on the gate voltage (top or bottom). It is possible that the ALD process affected the AlN shell in some manner that increased surface state density and depleted the NWs.

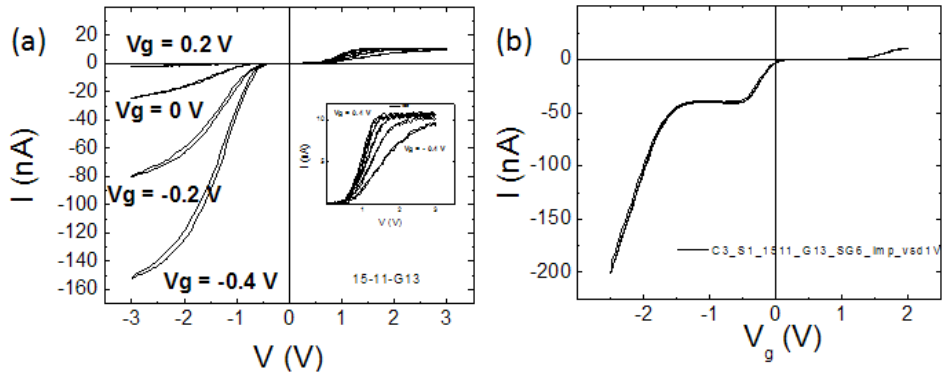

Figure 15. I-V characteristics for top Schottky-gate FETs

3.7 Theoretical modeling of the electronic structure of & electron gas formation in core-shell NWs

The overall goal of the LDRD project is to explore the possibility of creating a quasi-one-dimensional electron gas at the core/shell heterojunction. Experimentally, the set of parameters is large: core size, shell thickness, core and shell doping, materials for the core and shell. The goal of the modeling work is threefold: (1) to explore the parameter space and identify the conditions under which a 1DEG or 2DEG might be expected; (2) to understand the detailed electronic properties of the electron gas; (3) to model in detail the properties of the particular structures realized experimentally.

Initially, we developed a self-consistent approach to model the core/shell NWs and explored the parameter space that leads to a Q1D electron gas. This model considered the electronic structure of the two materials that form the core and shell to be simply those of the bulk materials. One important conclusion that was reached at the end of the first year is that at these dimensions one cannot neglect quantization effects that strongly modify the electronic structure. As a consequence, we subsequently extended our modeling capabilities so that the electronic structure of the core/shell NW became an explicit part of the self-consistent scheme. Thus, we now have a self-consistent Poisson-Schrödinger approach applicable to any core/shell NW geometry, including the triangular geometry relevant to current experiments in this project. This flexibility in the geometry arises because we are now solving Poisson's equation using a finite-element technique. Finally, we included polarization effects which are important to and specific to the III-nitride materials. These include the spontaneous polarization and the piezoelectric polarization. To include the latter we solved the mechanical equilibrium equations to obtain the strain in the core/shell NWs via finite element modeling, and then used these results to calculate the piezoelectric polarization in the Poisson-Schrödinger solver.

The overall approach works in the following steps:

1. Set-up the parameters for the core/shell NW
2. Obtain the finite-element mesh
3. Obtain the strain fields
4. Guess an input charge distribution
5. Calculate the electrostatic potential by solving Poisson's equation on the finite-element mesh
6. Calculate the charge from the electrostatic potential by solving Schrödinger's equation in an effective mass representation
7. Add the polarization charge
8. Go back to 4, exit when charge and potential are self-consistent

To illustrate the results that are obtained from this technique, Figure 16 shows an example for a GaN/$Al_xGa_{(1-x)}N$ NW for which the parameters were chosen to match those of the experimentally synthesized NWs. In this case the core radius is 100 nm and the shell thickness is 15nm. The $Al_xGa_{(1-x)}N$ composition is x=0.3. For these calculations polarization effects were not included in order to better judge their importance later.

Figure 16a shows the triangular cross-section and the finite-element mesh. The interesting result is shown in Figure 16b, where the self-consistent charge distribution in the NW is shown. Initially we had expected a uniform quasi-1DEG or 2DEG at the GaN/AlGaN interface, which we have previously calculated with core-shell NWs with cylindrical geometry. Instead, for the triangular NW geometry three quasi-1DEGs are formed at the corners of the triangle. This result is very interesting for a couple of reasons. First, even for a core as large as 100 nm we can still get quasi-1D behavior. Second, each of the electron gases at the three corners corresponds to a different wavefunction and thus we have three-fold degeneracy. This means that additional interactions such as piezoelectric effects, magnetic field effects, etc, can lift the degeneracy and lead to interesting electronic structure.

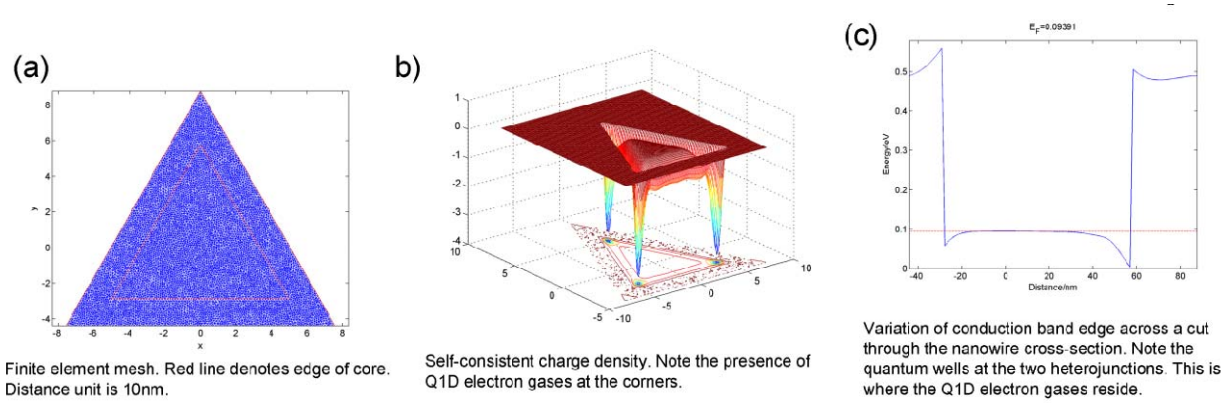

Figure 16. (a) Finite element mesh for core-shell $Al_{0.3}Ga_{0.7}N$/GaN NW with uniform doping of 2×10^{17} cm^{-3}; (b) calculated self-consistent charge and (c) potential for a triangular core-shell NW in the absence of polarization effects. The results indicate that three quasi-1DEGs are created at the corners.

The results discussed in Figure 16 serve to illustrate the role of nanoscale effects in influencing the type of electron gas that can be created in core-shell NWs. However, for the experimentally observed triangular wurtzite GaN NW geometry of there are strong polarization effects. The (0001) interface has strong spontaneous polarization, while the {1-101} interfaces are semi-polar. We thus included the spontaneous polarization on each of the faces in our self-consistent calculations, as shown in Figure 17.

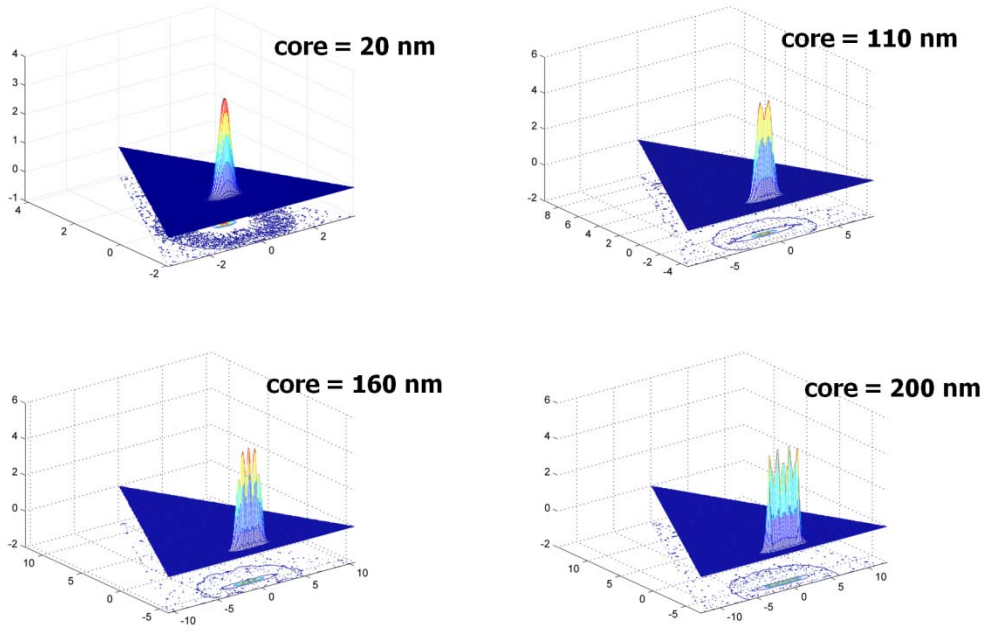

Figure 17. Calculated electron density in triangular core-shell NWs with spontaneous polarization.

With spontaneous polarization effects, the theoretical results indicate that a single quasi-1DEG gas is formed along the (0001) interface in contrast with the "non-polar" case where three 1DEGs were formed at the corners. In addition, we find that no hole gas forms at the two semi-polar faces, which have opposite spontaneous polarization to the (0001) face, because the n-type doping does not provide the hole free carriers to populate these interfaces. Future calculations of p-type doped NWs may reveal 1D hole gas (1DHG) formation. Another noteworthy aspect of Figure 17 is that the electron gas has a non-uniform density along the interface; this is a direct signature of quantum effects. For the NW with 20 nm core, only a single mode is occupied, which corresponds to the lowest energy state, and thus has only one maximum. As the core size is increased, more modes are being occupied, and the electron gas density shows several maxima.

In addition, we also investigated electron gas formation for both cases representing the {0001} facet of the NW as the Ga-polar (0001) (Ga terminated) or N-polar (000-1) (N terminated) face. The (0001) Ga-face and (000-1) N-face of GaN are nonequivalent and differ in their chemical and physical properties;*[22]* these two faces have opposite polarization signs and a 1DEG/2DEG is predicted to form only for the Ga-polar (0001) face for planar AlGaN/GaN

(0001) interfaces.*[23, 24]* While Ga-polar (0001) is generally observed for planar GaN growth, Qian et al recently reported the N-polar (000-1) face was observed in similar triangular GaN NWs, *suggesting that our NWs also contain the N-(000-1) and not Ga-(0001) face.[7]* As shown in Figure 18, the electron gas is located at the (0001) interface between the GaN core and the AlGaN shell. In contrast, when a {0001} facet is the N-polar (000-1) face an electron gas is still predicted to form; however it's location is near the opposite vertex. The origin of the 1DEG is likely from the two semi-polar {1-101} AlGaN/GaN facets, which for a planar case has the opposite polarization from the (000-1) face and correct polarization for electron gas formation.

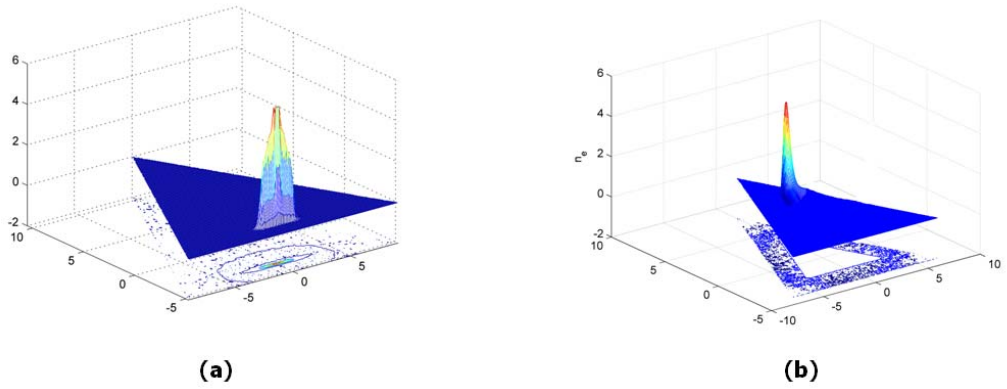

Figure 18. Electron densities for (a) GaN(0001) and (b) GaN(000-1) surfaces.

The next step in improving fidelity with experiment was to include piezoelectric polarization effects. To this end, we first obtained the relaxed strains in the core-shell AlGaN/GaN NW structure as shown in Figure 19. These strains were then used to calculate the piezoelectric polarization using the bulk values of the piezoelectric tensor.*[25]* We then re-computed the self-consistent charge and potential including this new contribution. Our results, shown at the bottom of Figure 19, suggest that piezoelectric polarization makes a minor contribution to the electron gas at the (0001) interface. A thicker AlGaN shell may potentially result in more strain, leading to more significant piezoelectric polarization effects, and this will be explored in future calculations.

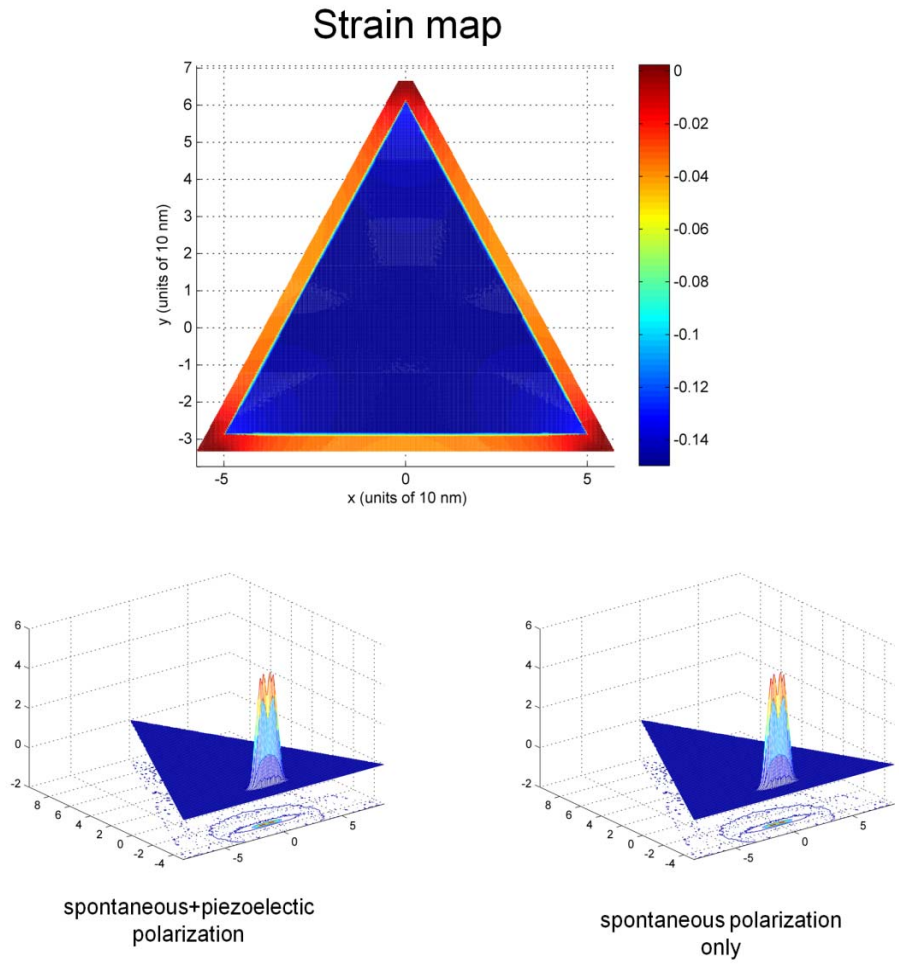

Figure 19. The top image shows the calculated strain fields inside of a GaN/AlGaN core-shell NW. The bottom images compare the electron density with and without the piezoelectric polarization included.

4. Conclusions & Future Work

In this work, III-nitride core-shell heterostructure NWs were investigated as model systems for studying the formation and physics of 1DEGs and 2DEGs in semiconductor nanostructures, as well as for understanding how surface and interface issues affect the electrical transport and optical properties of GaN NWs. GaN NWs as well as AlGaN/GaN and AlN/GaN core-shell NWs were synthesized and comprehensively studied using a battery of experimental techniques, including cross-section STEM, EDS, 3D STEM tomography, DLOS, ultrafast pump-probe measurements, electrical transport (I-V and FET) measurements, μ-PL, and spatially-resolved CL measurements. We note that studying the properties of these nanostructures is not

trivial, and often times not amenable to standard techniques to study planar III-nitride structures, and that many of our results represent the first successful application of these characterization techniques to III-nitride NWs or even core-shell NWs of any materials system. The experimental results show that the growth of AlN or AlGaN shell layers on GaN NWs has beneficial effects on electrical transport and optical properties, and suggest that the shell-layers passivate detrimental surface states.

Theoretical modeling was also performed in order to calculate the structure of electron gases formed in these novel NWs. Despite relatively large nanowire diameters, size quantization effects were observed with the formation of 1D electron gases in the AlGaN/GaN NWs. Spontaneous and piezoelectric polarization effects relevant to the III-nitrides were incorporated into our models. Calculations on NWs with either a Ga-face (0001) or N-face (000-1) revealed 1DEG formation in both cases for n-type NWs, although the position of the 1DEG was located at the vertex opposite the (000-1) AlGaN/GaN interface for the N-face case. In the future, we hope to examine the 1DEG/2DEG transition as a function of NW diameter, as well as explore additional parameters including p-type doping.

Our ultimate goal of conclusively demonstrating and studying the properties of 1DEGs and 2DEGs that might be formed in Al(Ga)N/GaN core-shell NWs has not yet been realized. While preliminary measurements on AlGaN/GaN NW FETs have shown improved conductivities and greatly enhanced mobilities over GaN FETs, it is not conclusive whether this is the result of 1DEG/2DEG formation or due to passivation of surface states that deplete carriers in the NWs. The potential lack of 1DEG/2DEG formation may be due to excessive defect states in the NWs, insufficient AlGaN thickness, heterointerface quality, and/or non-optimized contact and gate characteristics. Given further study and optimization efforts, we believe electron gas formation in these novel structures is inevitable; this assertion is bolstered by the theoretical predictions and a recent report claiming electron gas formation in AlGaN/AlN/GaN core-shell NWs.*[26]*

References

[1] G. Stan, C. V. Ciobanu, T. P. Thayer, G. T. Wang, J. R. Creighton, K. P. Purushotham, L. A. Bendersky, R. F. Cook, "Elastic moduli of faceted aluminum nitride nanotubes measured by contact resonance atomic force microscopy", *Nanotechnology*, ***20***, **2009**.

[2] I. Arslan, A. A. Talin, G. T. Wang, "Three-Dimensional Visualization of Surface Defects in Core-Shell Nanowires", *Journal of Physical Chemistry C*, ***112***, 11093 **2008**.

[3] Q. Li, G. T. Wang, "The Role of Collisions in the Aligned Growth of Vertical Nanowires", *J. Cryst. Growth (Netherlands)*, ***310***, 3706 **2008**.

[4] Q. Li, G. T. Wang, "Improvement in Aligned GaN Nanowire Growth using Submonolayer Ni Catalyst Films", *Appl. Phys. Lett.*, ***93***, 043119 **2008**.

[5] G. T. Wang, A. A. Talin, D. J. Werder, J. R. Creighton, E. Lai, R. J. Anderson, I. Arslan, "Highly aligned, template-free growth and characterization of vertical GaN nanowires on sapphire by metal-organic chemical vapour deposition", *Nanotechnology*, ***17***, 5773 **2006**.

[6] A. A. Talin, G. T. Wang, E. Lai, R. J. Anderson, "Correlation of growth temperature, photoluminescence, and resistivity in GaN nanowires", *Appl. Phys. Lett.*, ***92***, 093105 **2008**.

[7] F. Qian, Y. Li, S. Gradecak, H.-G. Park, Y. Dong, Y. Ding, Z. L. Wang, C. M. Lieber, "Multi-quantum-well nanowire heterostructures for wavelength-controlled lasers", *Nature Mater. (UK)*, ***7***, 701 **2008**.

[8] A. A. Talin, F. Leonard, B. S. Swartzentruber, X. Wang, S. D. Hersee, "Unusually strong space-charge-limited current in thin wires", *Phys. Rev. Lett. (USA)*, ***101***, **2008**.

[9] R. Calarco, M. Marso, T. Richter, A. I. Aykanat, R. Meijers, A. V. Hart, T. Stoica, H. Luth, "Size-dependent photoconductivity in MBE-grown GaN - Nanowires", *Nano Lett.*, ***5***, 981 **2005**.

[10] C. Donolato, "On the theory of SEM charge-collection imaging of localized defects in semiconductors", *Optik*, ***52***, 19 **1978**.

[11] C. E. Norman, "Challenging the spatial resolution limits of CL and EBIC", presented at *Diffusion and Defect Data Part B (Solid State Phenomena)*, Switzerland, 2001, **2001**.

[12] G. Anders, P. Mats-Erik, M. Lars, S. Lars, Vol. 84, AIP, **1998**, 1715.

[13] A. Chantre, G. Vincent, D. Bois, "Deep-level optical spectroscopy in GaAs", *Phys. Rev. B, Condens. Matter (USA)*, ***23***, 5335 **1981**.

[14] A. Armstrong, Q. Li, K. H. A. Bogart, Y. Lin, G. T. Wang, "Deep level optical spectroscopy investigation of GaN nanorods", *J. Appl. Phys. (USA)*, ***106***, 053712 **2009**.

[15] A. Hierro, D. Kwon, S. A. Ringel, M. Hansen, J. S. Speck, U. K. Mishra, S. P. DenBaars, "Optically and thermally detected deep levels in n-type Schottky and p(+)-n GaN diodes", *Appl. Phys. Lett.*, ***76***, 3064 **2000**.

[16] P. B. Klein, J. A. Freitas, Jr, S. C. Binari, A. E. Wickenden, "Observation of deep traps responsible for current collapse in GaN metal-semiconductor field-effect transistors", *Appl. Phys. Lett.*, ***75***, 4016 **1999**.

[17] T. B. Norris, K. Kim, J. Urayama, Z. K. Wu, J. Singh, P. Bhattacharya, "Density and temperature dependence of carrier dynamics in self-organized InGaAs quantum dots", *J. Phys. D: Appl. Phys.*, ***38***, 2077 **2005**.

[18] G. T. Wang, A. A. Talin, D. J. Werder, J. R. Creighton, E. Lai, R. J. Anderson, I. Arslan, "Highly aligned, template-free growth and characterization of vertical GaN nanowires on sapphire by metal-organic chemical vapour deposition", *Nanotechnology*, ***17***, 5773 **2006**.

[19] M. A. Reshchikov, H. Morkoc, "Luminescence properties of defects in GaN", *J. Appl. Phys.*, ***97***, 061301 **2005**.
[20] P. C. Upadhya, Q. Li, G. T. Wang, A. J. Fischer, A. J. Taylor, R. P. Prasankumar, "The influence of defect states on non-equilibrium carrier dynamics in GaN nanowires", *Semiconductor Science and Technology*, **Submitted**.
[21] A. A. Talin, G. T. Wang, E. Lai, R. J. Anderson, "Correlation of growth temperature, photoluminescence, and resistivity in GaN nanowires", *Appl. Phys. Lett.*, ***92***, 093105 **2008**.
[22] E. S. Hellman, "The polarity of GaN: a critical review", *MRS Internet J. Nitride Semicond. Res.*, ***3***, 1 **1998**.
[23] A. E. Romanov, T. J. Baker, S. Nakamura, J. S. Speck, E. J. U. Grp, "Strain-induced polarization in wurtzite III-nitride semipolar layers", *J. Appl. Phys. (USA)*, ***100***, **2006**.
[24] O. Ambacher, B. Foutz, J. Smart, J. R. Shealy, N. G. Weimann, K. Chu, M. Murphy, A. J. Sierakowski, W. J. Schaff, L. F. Eastman, R. Dimitrov, A. Mitchell, M. Stutzmann, "Two dimensional electron gases induced by spontaneous and piezoelectric polarization in undoped and doped AlGaN/GaN heterostructures", *J. Appl. Phys. (USA)*, ***87***, 334 **2000**.
[25] F. Bernardini, V. Fiorentini, D. Vanderbilt, "Spontaneous polarization and piezoelectric constants of III-V nitrides", *Phys. Rev. B*, ***56***, 10024 **1997**.
[26] Y. Li, J. Xiang, F. Qian, S. Gradecak, Y. Wu, H. Yan, H. Yan, D. A. Blom, C. M. Lieber, "Dopant-free GaN/AlN/AlGaN radial nanowire heterostructures as high electron mobility transistors", *Nano Lett.*, ***6***, 1468 **2006**.

Appendix – List of Publications Resulting from this Work

Refereed Publications:

[1] A. Armstrong, Q. Li, Y. Lin, G. T. Wang, A. A. Talin, "GaN nanowire surface state observed using deep level optical spectroscopy", *in preparation.*

[2] Y. Lin, Q. Li, A. Armstrong, G. T. Wang, "In situ scanning electron microscope electrical characterization of GaN nanowire nanodiodes using tungsten and tungsten/gallium nanoprobes", *Solid State Commun.*, ***149***, 1608 **2009**.

[3] I. Arslan, A. A. Talin, G. T. Wang, "Three-Dimensional Visualization of Surface Defects in Core-Shell Nanowires", *J. of Phys. Chem. C*, ***112***, 11093 **2008**.

[4] Q. Li, G. T. Wang, "The Role of Collisions in the Aligned Growth of Vertical Nanowires", *J. Cryst. Growth*, ***310***, 3706 **2008**.

[5] Q. Li, G. T. Wang, "Improvement in Aligned GaN Nanowire Growth using Submonolayer Ni Catalyst Films", *Appl. Phys. Lett.*, ***93***, 043119 **2008**.

[6] A. A. Talin, F. Leonard, B. S. Swartzentruber, X. Wang, S. D. Hersee, "Unusually strong space-charge-limited current in thin wires", *Phys. Rev. Lett. (USA)*, ***101***, **2008**.

[7] A. A. Talin, G. T. Wang, E. Lai, R. J. Anderson, "Correlation of growth temperature, photoluminescence, and resistivity in GaN nanowires", *Appl. Phys. Lett.*, ***92***, 093105, **2008**.

[8] L. Baird, G. H. Ang, C. H. Low, N. M. Haegel, A. A. Talin, Q. Li, G. T. Wang, "Imaging minority carrier diffusion in GaN nanowires using near field optical microscopy," *Phys. B*, accepted.

[9] Q. Li and G. T. Wang, "Surface-related yellow luminescence in GaN nanowires revealed by high resolution cathodoluminescence," *in preparation.*

[10] G. T. Wang, Q. Li, A. A. Talin, A. Armstrong, Y. Lin, J. Huang, "GaN Nanowires: Growth, Characterization, and Applications," *ECS Transactions*, 19 (8) 55-61, **2009**

Distribution List

Copies	Mailstop	Recipient	Org.
1	MS1086	George T. Wang	01126
1	MS1086	Robert M. Biefeld	01126
1	MS9161	Francois Leonard	08656
1	MS1421	Jerry A. Simmons	01130
1	MS1421	Jeffrey Y. Tsao	01120
1	MS1086	Qiming Li	01126
1	MS1086	Michael E. Coltrin	01126
1	MS9403	Bryan Wong	08223
1	MS0899	Technical Library (electronic copy)	9536
1	MS0123	D. Chavez, LDRD Office	01011